Author Manuscript
Author Manuscript
Author Manuscript
Author Manuscript

HHS Public Access
Author manuscript
ACS Nano. Author manuscript; available in PMC 2024 March 13.

Published in final edited form as:
ACS Nano. 2023 December 26; 17(24): 24936–24946. doi:10.1021/acsnano.3c06577.

Ultrasound-Induced Cascade Amplification in a Mechanoluminescent Nanotransducer for Enhanced Sono-Optogenetic Deep Brain Stimulation

Wenliang Wang,
Biomedical Engineering Cockrell School of Engineering, The University of Texas at Austin, Austin, Texas 78712, United States

Kai Wing Kevin Tang,
Biomedical Engineering Cockrell School of Engineering, The University of Texas at Austin, Austin, Texas 78712, United States

Ilya Pyatnitskiy,
Biomedical Engineering Cockrell School of Engineering, The University of Texas at Austin, Austin, Texas 78712, United States

Xiangping Liu,
Biomedical Engineering Cockrell School of Engineering, The University of Texas at Austin, Austin, Texas 78712, United States

Xi Shi,
Department of Molecular Biosciences, The University of Texas at Austin, Austin, Texas 78712, United States

David Huo,

Corresponding Author Huiliang Wang – Biomedical Engineering Cockrell School of Engineering, The University of Texas at Austin, Austin, Texas 78712, United States; evanwang@utexas.edu.

Author Contributions
W.W., K.T., I.P., and X.L. contributed equally to this work.

EXPERIMENTAL SECTION/METHODS
The experimental details and all characterization are shown in the Supporting Information. pGP-CMV-NES-jRGECO1a was a gift from Douglas Kim & GENIE Project (Addgene plasmid # 61563; http://n2t.net/addgene:61563; RRID:Addgene_61563). pAAV.Syn.NES-jRGECO1a.WPRE.SV40 was a gift from Douglas Kim & GENIE Project (Addgene viral prep # 100854-AAV9; http://n2t.net/addgene:100854; RRID:Addgene_100854); pAAV-hSyn-hChR2-(H134R)-EYFP was a gift from Karl Deisseroth (Addgene viral prep # 26973-AAV9; http://n2t.net/addgene:26973; RRID:Addgene_26973). Thy1-ChR2-YFP transgenic mice and C57BL/6J wild-type mice were ordered from the Jackson Laboratory. All procedures were designed according to the National Institute of Health Guide for the Care and Use of Laboratory Animals, approved by the Institutional Animal Care and Use Committee at the University of Texas at Austin, and were supported via the Animal Resources Center at the University of Texas at Austin.

The authors declare the following competing financial interest(s): The authors declare that a patent application relating to this work has been filed.

Supporting Information
The Supporting Information is available free of charge at https://pubs.acs.org/doi/10.1021/acsnano.3c06577.
Tracking of neuron spiking under sono-optogenetics (MP4)
Contralateral left limb motion in mice under sono-optogenetics(MP4)
Remote VTA neuron activation through sono-optogenetics for lever press tests (MP4)
Materials and instruments, experimental methods, fluorescence spectra, XRD, DLS tests of nanotransducers, UV–vis spectra, light emission detection of nanotransducers, heat map of ultrasound energy transmission in the mouse head, confocal images, lever press testing system photograph, H&E staining, biosafety evaluation, and antibody information (PDF)

Author Manuscript Author Manuscript Author Manuscript Author Manuscript

Biomedical Engineering Cockrell School of Engineering, The University of Texas at Austin, Austin, Texas 78712, United States

Jinmo Jeong,
Biomedical Engineering Cockrell School of Engineering, The University of Texas at Austin, Austin, Texas 78712, United States

Thomas Wynn,
Biomedical Engineering Cockrell School of Engineering, The University of Texas at Austin, Austin, Texas 78712, United States

Arjun Sangani,
Biomedical Engineering Cockrell School of Engineering, The University of Texas at Austin, Austin, Texas 78712, United States

Andrew Baker,
Biomedical Engineering Cockrell School of Engineering, The University of Texas at Austin, Austin, Texas 78712, United States

Ju-Chun Hsieh,
Biomedical Engineering Cockrell School of Engineering, The University of Texas at Austin, Austin, Texas 78712, United States

Anakaren Romero Lozano,
Biomedical Engineering Cockrell School of Engineering, The University of Texas at Austin, Austin, Texas 78712, United States

Brinkley Artman,
Biomedical Engineering Cockrell School of Engineering, The University of Texas at Austin, Austin, Texas 78712, United States

Lief Fenno,
Department of Psychiatry & Behavioral Science, The University of Texas at Austin Dell Medical School, Austin, Texas 78712, United States

Vivek P. Buch,
Department of Neurosurgery, Stanford University, Stanford, California 94304, United States

Huiliang Wang
Biomedical Engineering Cockrell School of Engineering, The University of Texas at Austin, Austin, Texas 78712, United States

Abstract

Remote and genetically targeted neuromodulation in the deep brain is important for understanding and treatment of neurological diseases. Ultrasound-triggered mechanoluminescent technology offers a promising approach for achieving remote and genetically targeted brain modulation. However, its application has thus far been limited to shallow brain depths due to challenges related to low sonochemical reaction efficiency and restricted photon yields. Here we report a cascaded mechanoluminescent nanotransducer to achieve efficient light emission upon ultrasound stimulation. As a result, blue light was generated under ultrasound stimulation with a subsecond

Author Manuscript Author Manuscript Author Manuscript Author Manuscript

response latency. Leveraging the high energy transfer efficiency of focused ultrasound in brain tissue and the high sensitivity to ultrasound of these mechanoluminescent nanotransducers, we are able to show efficient photon delivery and activation of ChR2-expressing neurons in both the superficial motor cortex and deep ventral tegmental area after intracranial injection. Our liposome nanotransducers enable minimally invasive deep brain stimulation for behavioral control in animals via a flexible, mechanoluminescent sono-optogenetic system.

Graphical Abstract

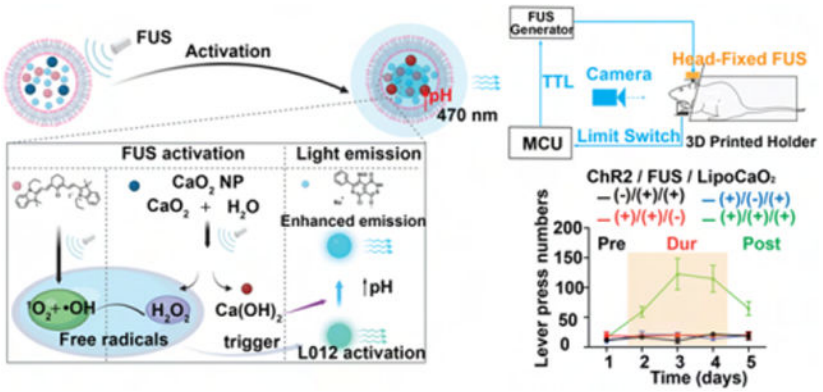

Keywords

focused ultrasound; optogenetics; lipids; sono-mechanoluminescence; neuromodulation

INTRODUCTION

Current electrical deep brain stimulation, while generally safe and effective, often exhibits a nonspecific tissue activation profile.[1,2] On the other hand, direct ultrasound could potentially also achieve noninvasive deep brain stimulation, but does not result in cell-type-specific neuromodulation within the brain.[1,2] This nonspecificity can potentially result in unwanted side effects stemming from the activation of nontarget tissues, ultimately limiting the therapy's efficacy.[1,2] Therefore, strategies to develop cell-type and circuit-specific deep brain stimulation could be an approach to optimize targeted neuromodulation therapy. Optogenetics is a powerful tool for achieving precise control of specific types of neurons and circuits to understand brain structure in health and disease.[3-6] However, clinical application of this technology is restricted by invasive light delivery requirements in larger brain volumes.[3,7] Remote and genetically targetted neural modulation in deep brain regions is a promising approach to the advent of clinical applications. More recently, opsins, including ChRmine[8] and step-function opsin,[9,10] and near-infrared (NIR) light-based genetics with nanoparticles[7,11] have enabled less invasive neuronal modulation in mice. However, the intrinsic limitation of light penetration depth in brain tissue continues to be one of the main limiting factors for its application in nonhuman primates and humans. Moreover, X-ray-activated luminescent nanoparticles have been designed for remote and minimally invasive optogenetics, but the damage to tissues by X-ray radiation must be considered.[12,13] As alternatives to visible/NIR light and X-ray radiation with excellent penetration performance

Author Manuscript Author Manuscript Author Manuscript Author Manuscript

and safety profiles are magnetic field and focused ultrasound (FUS). Magnetic modulation with nanotransducers[14-16] and sonogenetic modulation by combining ultrasound with mechanosensitive ion channels[17-22] have been shown to function in deep neuronal tissue. Magnetic modulation approaches are generally slow, hypothesized to be due to latency in converting magnetic power to heating or mechanical force, which hampers their application in fast control of neuronal activity.[11,18,23-27] On the other hand, while great progress has been reported in sonogenetics, the programmability of sonogenetics is still limited with respect to neural excitation in comparison to the comprehensive optogenetics toolbox that enables versatile control of neuronal excitation, inhibition, excitability, and precise activation frequency/kinetics.[18,19,28,29] Therefore, it is most desirable to develop a minimally invasive and remote light delivery technology that could utilize the optogenetic toolbox for neuroscience research and clinical applications.

Utilizing nanoparticles converting ultrasound energy to light has become an increasingly promising technology for combining noninvasive and clinically safe ultrasound technology with an optogenetic toolbox for neuromodulation.[30-36] The initial application of sono-optogenetics, which involved rechargeable inorganic mechanoluminescent colloidal solutions for ultrasound-to-light conversion, successfully demonstrated ChR2-expressing neuron activation in the motor cortex of mice but was constrained by increased engineering complexity.[37-41] We have recently designed a simpler and more biocompatible liposomal nanolight source triggered by FUS.[42] However the current sono-mechanoluminescent systems exhibit limited photon yields, which restricts their ability to activate neurons only in shallow brain regions. The practical application of mechanoluminescent materials in optogenetics necessitates the ability to temporally control light emission and achieve high photon yields in the solution.[40] While significant progress has been made in the field of mechanoluminescence, the current reported materials predominantly emit light in bulk form through piezoelectric effects and cycloreversions.[34] Moreover, the lack of temporal control of light emission exhibited by these sono-mechanoluminescent systems further diminishes their suitability for optogenetics applications.[35,43] Therefore, the development of an efficient mechanoluminescent system with enhanced brightness and transient light control capability is crucial for enabling the application of sono-optogenetics in deeper tissues.

In this work, we developed a strategy to rectify current limitations of mechanoluminescent nanoparticles to enable sono-optogenetic deep brain stimulation. We developed cascaded sono-optogenetics with high ultrasound sensitivity and spatiotemporal resolution to achieve temporal activation of neurons at both the superficial motor cortex and the deep brain ventral tegmental area (VTA) after intracranial injection (Figure 1a). In brief, chemiluminescence L012, sonosensitizer IR780, and sono-amplifier polyethylene glycol (PEG) 200 coated calcium peroxide (CaO_2) nanoparticles were loaded into lipids to prepare a nano light transducer for opsin activation under FUS stimulation. Free radicals generated by IR780 after absorbing ultrasound energy can activate L012 to emit a blue light. Meanwhile, the alternating ultrasound pressure wave will perturb the liposome membrane and PEG coating at the surface of CaO_2, thus enabling the reaction of CaO_2 and water to produce hydrogen peroxide (H_2O_2) and calcium hydroxide ($Ca(OH)_2$), increasing the local concentration of free radicals and pH. Since L012 reactivity may be inhibited by protonation of the luminol molecule at low pH values,[44] the increased pH and free radical concentration are expected

Author Manuscript Author Manuscript Author Manuscript Author Manuscript

to improve the quantum yield of L012 (Figure 1b). We evaluated *in vivo* light emission and optogenetic neuronal stimulation and found low activation latency, even at a depth of 5 mm, hence achieving minimally invasive, spatiotemporal sono-optogenetic control of neuronal activity in the deep mouse brain.

RESULTS AND DISCUSSION

In our recent work, ultrasound-triggered cascade reactions in Lipo@IR780/L012 liposomes achieved synchronized and stable blue light emission, but the limited light emission intensity was not enough to achieve deep brain stimulation.[42] In fact, the local free radical concentration and pH in liposomes both play crucial roles in the light emission power. As shown in Figure S1, the fluorescence intensity of L012 increased by around 30% when the pH changed from 7.4 to 10 and improved around four times when the H_2O_2 concentration was increased from 50 to 500 μM.[44,45] To achieve improved light emission intensity under ultrasound irradiation, sono-amplifier PEG_{200} coated CaO_2 nanoparticles were first prepared by a calcium chloride ($CaCl_2$)–hydrogen peroxide (H_2O_2) reaction in PEG_{200} solution.[46] The specific peaks (2θ = 30.1°, 35.7°, 47.4°, and 53.3°) of CaO_2 are clearly shown in the X-ray diffraction spectrum (Figure 1c), and the transmission electron microscope (TEM) results determined that these nanoparticles have 18 ± 12 nm diameters (Figure 1d). X-ray diffraction results showed that the CaO_2 nanoparticles have high stability (Figure S2) in solution but rapidly reacted with water to form H_2O_2 and $Ca(OH)_2$ (Figure 1e, 2θ = 29.4° and 35.6°) once exposed to ultrasound irradiation. The reaction between CaO_2 nanoparticles and water scarcely occurred in the absence of ultrasound due to the protective effects of the PEG coating layers on the CaO_2 nanoparticles. However, this reaction was accelerated by ultrasound stimulation. The $Ca(OH)_2$ formed would dissolve in the solution, releasing OH^- ions and subsequently increasing the local pH within the liposome.[47] Our L012, IR780, and CaO_2-loaded liposomes were then prepared using a thin film hydration strategy,[48,49] and their TEM images are shown in Figure 1f. The dynamic scattering tests (DLS) determined that the liposome size slightly increased to 175.9 ± 0.9 nm after payload loading (Figure 1g and Table 1) compared with blank liposomes, and the negative surface zeta potential guaranteed the stability of liposomes in tissue fluid (Figure 1h and Table 1). The DLS results indicated a slight increase in the size of the nanoparticles and a slight broadening of the size distribution after ultrasound stimulation (Figure S3). This might be attributed to the consumption of CaO_2 upon contact with water during ultrasound exposure, potentially leading to destabilization of the liposome membrane and an increase in membrane fluidity, thereby resulting in the observed changes in size and distribution. The drug loading capacity (DLC) of IR780 and L012 in the liposomes was 5.7 and 6.2 wt %, respectively, determined via UV–vis spectroscopy (Table 1). The L012/CaO_2 weight ratio of 1:5 was used in all of the following experiments. The DLC of CaO_2 in the liposomes was 2.8 wt % measured via inductively coupled plasma mass spectrometry (ICP-MS).

Ultrasound-triggered cascade reactions dominate the spatiotemporal light emission from these Lipo@IR780/L012/CaO_2 liposomes, where the generation of free radicals including singlet oxygen ($^1O_2$), hydroxyl radical ($^{\bullet}OH$), and H_2O_2 is first necessary to activate nearby L012 under the irradiation. Thus, we first evaluated the generation of these free radicals in Lipo@IR780/CaO_2 liposomes via different free radical probes. Singlet oxygen ($^1O_2$) and

Author Manuscript Author Manuscript Author Manuscript Author Manuscript

hydroxyl radical ($^{\bullet}OH$) were the main free radical species from IR780 under ultrasound irradiation.[42] 1,3-Diphenylisobenzofuran (DPBF) was used to detect $^1O_2$ generation due to its highly specific reactivity.[42,50] As shown in Figure 2a, the characteristic UV–vis absorption peak of DPBF at 420 nm (blue arrow) sharply decreased with ultrasound irradiation time to form 1,2-dibenzoylbenzene (DBB). Still, no apparent changes were observed when ultrasound irradiation was off (Figure S4a). The quantification determined that more than 20% DPBF was consumed via Lipo@IR780/CaO_2 liposomes in comparison to Lipo@IR780 liposomes after 60 s of FUS irradiation, but no changes occurred without FUS irradiation (Figure 2b). Then, we also evaluated the generation of $^{\bullet}OH$ and H_2O_2 by measuring the decomposition of salicylic acid (SA). The SA would rapidly react with $^{\bullet}OH$ and H_2O_2 to form 2,3-dihidroxybenzoic acid and 2,5-dihydroxibenzoic acid.[42,51,52] As shown in Figure 2c and Figure S4b, the characteristic UV–vis absorption peak of SA at 297 nm (blue arrow) dramatically decreased with FUS irradiation time, and no changes were observed without FUS. The quantification showed a decomposition of SA by more than 10% by Lipo@IR780/CaO_2 liposomes in comparison to Lipo@IR780 liposomes after 60 s of FUS irradiation. We next evaluated free radical production at different ultrasound powers. As shown in Figure S4c and Figure S4d, the free radical concentration increased with ultrasound energy, with the Lipo@IR780/CaO_2 liposomes exhibiting higher ultrasound sensitivity and free radical production yield compared with Lipo@IR780. Finally, L012 is a potent free radical scavenger, and we expected that the free radicals could be temporally quenched via L012 to produce light instead of leaking out to damage nearby cells. Thus, we also examined if free radicals were released from the Lipo@IR780/L012/CaO_2 liposomes and the results showed that no free radical residues were released outside of the liposomes after the FUS irradiation (Figure 2e,f and Figure S4e,f).

Next, we investigated the ultrasound-triggered mechanoluminescence performance of Lipo@IR780/L012/CaO_2 liposomes (Figure 3a). The cascade reactions, including free radical generation and quenching, dominated this ultrasound-triggered mechanoluminescence. Free radicals could be generated and quenched for light emission within 5.5 and 28 μs, respectively, owing to the high reaction rate constant (4.5×10^{-5} M^{-1} s^{-1}, 2.67×10^{-8} M^{-1} s^{-1}).[53,54] Theoretically, light will be generated within 33.5 μs once the liposomes are stimulated via FUS. Time-resolved sono-mechanoluminescence spectra showed that synchronous photons were produced following the FUS pulse, where the delay time of light emission was less than 4 ms, even at 10 Hz stimulation (Figures 3b, 3c and S5 and S6), which is shorter than the time-to-spike latency of approximately 10 ms for ChR2 neuron activation.[55] In addition, we evaluated ultrasound power-dependent light emission, as shown in Figure 3d and Figure S7. Lipo@IR780/L012/CaO_2 liposomes exhibited higher photon productivity and ultrasound sensitivity compared with Lipo@IR780/L012. Next, we investigated the ultrasound-triggered photon delivery performance in tissue. Ultrasound energy propagates through tissue as a traveling pressure wave, exponentially attenuating with tissue depth.[56,57] As shown in Figure 3e, the ultrasound wave of 1.5 MHz could achieve a penetration of 20 mm with 40% energy delivered even at a tissue depth of 10 mm. The energy transfer efficiency of ultrasound is orders of magnitude higher than both visible and NIR light.[7,8,58] Furthermore, Lipo@IR780/L012/CaO_2 liposomes demonstrated higher ultrasound-triggered photon production at a comparable tissue depth compared to

Author Manuscript Author Manuscript Author Manuscript Author Manuscript

Lipo@IR780/L012 liposomes. Photon production exhibited a decrease with increasing tissue depth, but noteworthy light generation was still observed even at a depth of 10 mm (Figure 3f and Figure S8). These data demonstrated the potential for achieving remote and wireless photon delivery for minimally invasive brain modulation.

Next, we investigated opsin activation in primary neuron cultures under sono-mechanoluminescent irradiation. The mechanoluminescence spectra of Lipo@IR780/L012/CaO_2 liposomes exhibited the maximal emission wavelength at around 470 nm, and the photon yield was about three times higher than that of Lipo@IR780/L012 liposomes (Figure 3g). The light emission wavelength mainly overlapped with the channelrhodopsin-2 (ChR2) for optogenetic stimulation.[59] JRGECO1a red calcium indicators were chosen to track neuron activity and minimize spectral overlap (Figure 3h and Movie S1).[60,61] Neurons transduced with AAV9-hSyn::ChR2-EYFP and AAV9-hSyn::NES-JRGECO1a (Figure 3i) exhibited synchronized firing after the irradiation in the presence of ultrasound (FUS+) and Lipo@IR780/L012/CaO_2 liposomes (LipoCaO_2+) with around 80% spike probability, but no evident increase of calcium fluorescence was observed in all other control groups (Figure 3j-l).

We next tested sono-optogenetic neural activation in the mouse secondary motor cortex (M2), where optogenetic activation is expected to modulate limb motion. Local injection is chosen in this work due to higher spatial resolution, higher emission intensity, and prolonged stability for multiple days' stimulation, especially important for VTA described later. Here, the Lipo@IR780/L012/CaO_2 liposomes were unilaterally injected into the right M2 of Thy1-ChR2-YFP transgenic mice. After 24 h, FUS was applied to the M2 region of the mouse brain (Figure 4a). The normalized ultrasound energy heat map at the mouse motor cortex showed that around 1.15 MPa peak pressure was delivered to the M2 region when 1.55 MPa primary ultrasound energy was used (Figure S9). The high energy transfer efficiency ensured that these liposomes could be effectively activated. As shown in Figure 4b, the synchronous blue light with power intensity 1.21 mW/mm^2 was generated under the FUS stimulation, which should be sufficient to achieve more than 60% wild-type ChR2 spike probability.[8,62] Furthermore, it is worth noting that the ultrasound's thermal effect can activate neurons through temperature-sensitive ion channels.[63,64] Therefore, we assessed the local temperature at the targeted brain area during sono-optogenetic stimulation. Our findings revealed a mere 1.0 °C increase during the 20 s ultrasound stimulation, with no significant intracranial heating observed that could potentially alter neuronal physiology (Figure S10). Since the motor cortex is responsible for higher-order control of movement,[65] we tested *in vivo* sono-optogenetic stimulation in anesthetized subjects by video tracking of contralateral and ipsilateral limbs (Figure 4a). As shown in Figure 4c,d and Movie S2, DeepLabCut analysis determined that contralateral left limb motion was observed in Thy1-ChR2-YFP transgenic mice with FUS stimulation with liposome injection, while no ipsilateral limb motion was observed. Limb motion was not activated in the absence of FUS stimulation or liposome injection, or in wild-type mice. We anticipate seeing some limb motion in wild-type mice with FUS stimulation of endogenous mechanosensitive ion channels and anticipate the absence such nonspecific activity is a result of anesthesia.[66-69] We next evaluated neuron activation in *posthoc* tissue samples via expression of immediate early gene marker c-Fos. A dramatic increase in c-Fos signals was selectively observed

Author Manuscript Author Manuscript Author Manuscript Author Manuscript

in the right M2 region in subjects receiving both FUS stimulation and liposome injection (Figure 4f,g and Figure S11). These results suggested that sono-optogenetics with our liposome nanotransducers is sufficient to achieve effective, remote, and minimally invasive photon delivery in the motor cortex for neuron activation.

Finally, we investigated ultrasound-triggered deep photon delivery in the mouse VTA. The VTA is well-known for regulating both motor behavior and reward learning via dopaminergic projections.[70,71] We chose to assay the function of our sono-optogenetic approach in a head-fixed, lever pressing paradigm, which allows the animal to activate the ultrasound trigger (Figure 5a and Figure S12). Before behavioral evaluation, we first assayed ultrasound-driven *in vivo* light emission at the VTA (1.5 MHz, 1.55 MPa, pulse 100 ms on, 900 ms off). Due to the high energy transfer efficiency of ultrasound in brain tissue, around 0.97 MPa of ultrasound energy from 1.55 MPa of primary ultrasound source was measured at the VTA, which is sufficient to activate liposomal light emission (Figure S13). The time-resolved light emission spectra showed that temporal blue light of 1.0 mW/mm^2 power density was detected under ultrasound stimulation (Figure 5b), which is sufficient to activate ChR2-expressing neurons. Liposomes were unilaterally injected into the mouse VTA region, and an ultrasound stimulation metal ring was affixed to the skull. Twenty-four hours after surgery, the mouse was placed in the 3D-printed holder allowing the animal to reach the ultrasound-triggering lever with the front limbs. Upon pressing the lever, the FUS transducer was programmed to generate one pulse (100 ms on, 1.5 MHz, 1.55 MPa). To systematically investigate the reward-seeking behaviors under sono-optogenetics, we tracked the mouse press number over 5 days, including prestimulus (Pre, the FUS pulse is always off) at day 1, during stimulation (Dur, a FUS pulse was generated once the mouse presses the lever) at day 2 to day 4, and poststimulus (Post, the FUS pulse is always off) at day 5. Mice were not observed to have an innate preference for lever pressing (Figure 5c). However, the Thy1-ChR2-YFP transgenic mice administered both liposomes and FUS stimulation exhibited rapidly increased lever pressing rates with FUS (Dur), and this preference was preserved across trial days, as observed with continued lever pressing without FUS stimulation (Post) (Figure 5d-g, and Movie S3). We again evaluated expression of c-Fos (Figure 5h,i) and observed a significant increase in c-Fos signal under the Thy1-ChR2/FUS/liposome condition, including in tyrosine hydroxylase (TH)+ dopamine (DA) neurons. These results showcase the ability of our sono-optogenetic system to effectively deliver photons to the VTA, activate DA neurons, and achieve remote and minimally invasive modulation of reward learning behaviors. Finally, we investigated the *in vivo* biosafety and biocompatibility of this system. Seven days after sono-optogenetic stimulation, the brain sections stained with hematoxylin and eosin (H&E) showed that liposomes did not result in notable cell toxicity (Figure S14). We also noted no difference across samples in expression of glial activation (Iba1; Figure S15) or neuron apoptosis (caspase-3; Figure S16). Furthermore, these organic liposomes are expected to undergo brain clearance via the paravascular glymphatic pathway, wherein microglia intercept extraneous liposomes and facilitate their transportation to the paravascular regions for subsequent clearance.[72]

Author Manuscript Author Manuscript Author Manuscript Author Manuscript

CONCLUSION

In conclusion, we developed cascaded liposomal nanotransducers triggered by FUS to emit light for deep brain sono-optogenetics. Ultrasound energy can be noninvasively delivered to the deep brain via pressure waves with high transmission efficiency and subsequently sensed by the sonosensitizer IR780 and sono-amplifier CaO_2 to produce spatiotemporal blue light via a controlled cascade reaction in liposomes. *In vitro* and *in vivo* results suggested that ChR2-expressing neurons could be spatiotemporally controlled via irradiation by sono-mechanoluminescence, thus achieving temporal neuron activation at the motor cortex and VTA for behavioral modulation. Excellent biosafety and biocompatibility data make our sono-optogenetic system promising for minimally invasive, genetically targeted deep brain modulation in large animals in the future.

Supplementary Material

Refer to Web version on PubMed Central for supplementary material.

ACKNOWLEDGMENTS

TEM image acquisition was performed with the help of Michelle Mikesh at the Center for Biomedical Research Support Microscopy and Imaging Facility at UT Austin (RRID# SCR_021756). Dr. Huiliang Wang acknowledges funding support from the NIH Maximizing Investigators' Research Award (National Institute of General Medical Sciences 1R35GM147408), the University of Texas at Austin Startup Fund, a Robert A. Welsh Foundation grant (No. F-2084-20210327), and a Craig H. Neilsen Foundation Pilot Research grant. Dr. Jinmo Jeong acknowledges the Human Frontier Science Program Fellowship. We acknowledge BioRender.com for the figure drawings.

REFERENCES

(1). Cagnan H; Denison T; McIntyre C; Brown P Emerging Technologies for Improved Deep Brain Stimulation. Nat. Biotechnol 2019, 37, 1024–1033. [PubMed: 31477926]

(2). Ashkan K; Rogers P; Bergman H; Ughratdar I Insights into the Mechanisms of Deep Brain Stimulation. Nat. Rev. Neurol 2017, 13, 548–554. [PubMed: 28752857]

(3). Deisseroth K. Optogenetics: 10 Years of Microbial Opsins in Neuroscience. Nat. Neurosci 2015, 18, 1213–1225. [PubMed: 26308982]

(4). Kim CK; Adhikari A; Deisseroth K Integration of Optogenetics with Complementary Methodologies in Systems Neuroscience. Nat. Rev. Neurosci 2017, 18, 222–235. [PubMed: 28303019]

(5). Martorell AJ; Paulson AL; Suk H-J; Abdurrob F; Drummond GT; Guan W; Young JZ; Kim DN-W; Kritskiy O; Barker SJ; et al. Multi-Sensory Gamma Stimulation Ameliorates Alzheimer's-Associated Pathology and Improves Cognition. Cell 2019, 177, 256–271. [PubMed: 30879788]

(6). Etter G; van der Veldt S; Manseau F; Zarrinkoub I; Trillaud-Doppia E; Williams S Optogenetic Gamma Stimulation Rescues Memory Impairments in an Alzheimer's Disease Mouse Model. Nat. Commun 2019, 10, 5322. [PubMed: 31757962]

(7). Chen S; Weitemier AZ; Zeng X; He L; Wang X; Tao Y; Huang AJY; Hashimotodani Y; Kano M; Iwasaki H; et al. Near-Infrared Deep Brain Stimulation via Upconversion Nanoparticle-mediated Optogenetics. Science 2018, 359, 679–684. [PubMed: 29439241]

(8). Chen R; Gore F; Nguyen Q-A; Ramakrishnan C; Patel S; Kim SH; Raffiee M; Kim YS; Hsueh B; Krook-Magnusson E; et al. Deep Brain Optogenetics without Intracranial Surgery. Nat. Biotechnol 2021, 39, 161–164. [PubMed: 33020604]

(9). Yizhar O; Fenno LE; Prigge M; Schneider F; Davidson TJ; O'Shea DJ; Sohal VS; Goshen I; Finkelstein J; Paz JT; et al. Neocortical Excitation/inhibition Balance in Information Processing and Social Dysfunction. Nature 2011, 477, 171–178. [PubMed: 21796121]

Author Manuscript Author Manuscript Author Manuscript Author Manuscript

(10). Gong X; Mendoza-Halliday D; Ting JT; Kaiser T; Sun X; Bastos AM; Wimmer RD; Guo B; Chen Q; Zhou Y; et al. An Ultra-Sensitive Step-Function Opsin for Minimally Invasive Optogenetic Stimulation in Mice and Macaques. Neuron 2020, 107, 197. [PubMed: 32645306]

(11). Wu X; Jiang Y; Rommelfanger NJ; Yang F; Zhou Q; Yin R; Liu J; Cai S; Ren W; Shin A; et al. Tether-Free Photothermal Deep-Brain Stimulation in Freely Behaving Mice via Wide-Field Illumination in the near-Infrared-II Window. Nat. Biomed Eng 2022, 6, 754–770. [PubMed: 35314800]

(12). Chen Z; Tsytsarev V; Finfrock YZ; Antipova OA; Cai Z; Arakawa H; Lischka FW; Hooks BM; Wilton R; Wang D; et al. Wireless Optogenetic Modulation of Cortical Neurons Enabled by Radioluminescent Nanoparticles. ACS Nano 2021, 15, 5201–5208. [PubMed: 33625219]

(13). Matsubara T; Yanagida T; Kawaguchi N; Nakano T; Yoshimoto J; Sezaki M; Takizawa H; Tsunoda SP; Horigane S-O; Ueda S; et al. Remote Control of Neural Function by X-Ray-Induced Scintillation. Nat. Commun 2021, 12, 4478. [PubMed: 34294698]

(14). Bottomley PA; Andrew ER RF Magnetic Field Penetration, Phase Shift and Power Dissipation in Biological Tissue: Implications for NMR Imaging. Phys. Med. Biol 1978, 23, 630–643. [PubMed: 704667]

(15). Ouyang J; Tang Z; Farokhzad N; Kong N; Kim NY; Feng C; Blake S; Xiao Y; Liu C; Xie T; et al. Ultrasound Mediated Therapy: Recent Progress and Challenges in Nanoscience. Nano Today 2020, 35, 100949.

(16). Romero G; Park J; Koehler F; Pralle A; Anikeeva P Modulating Cell Signalling in Vivo with Magnetic Nanotransducers. Nature Reviews Methods Primers 2022, 2, 1–21.

(17). Ibsen S; Tong A; Schutt C; Esener S; Chalasani SH Sonogenetics Is a Non-Invasive Approach to Activating Neurons in Caenorhabditis Elegans. Nat. Commun 2015, 6, 8264. [PubMed: 26372413]

(18). Duque M; Lee-Kubli CA; Tufail Y; Magaram U; Patel J; Chakraborty A; Mendoza Lopez J; Edsinger E; Vasan A; Shiao R; et al. Sonogenetic Control of Mammalian Cells Using Exogenous Transient Receptor Potential A1 Channels. Nat. Commun 2022, 13, 600. [PubMed: 35140203]

(19). Liu T; Choi MH; Zhu J; Zhu T; Yang J; Li N; Chen Z; Xian Q; Hou X; He D; et al. Sonogenetics: Recent Advances and Future Directions. Brain Stimul. 2022, 15, 1308–1317. [PubMed: 36130679]

(20). Qiu Z; Kala S; Guo J; Xian Q; Zhu J; Zhu T; Hou X; Wong KF; Yang M; Wang H; et al. Targeted Neurostimulation in Mouse Brains with Non-Invasive Ultrasound. Cell Rep. 2020, 32, 108033. [PubMed: 32814040]

(21). Maresca D; Lakshmanan A; Abedi M; Bar-Zion A; Farhadi A; Lu GJ; Szablowski JO; Wu D; Yoo S; Shapiro MG Biomolecular Ultrasound and Sonogenetics. Annu. Rev. Chem. Biomol. Eng 2018, 9, 229–252. [PubMed: 29579400]

(22). Cadoni S; Demené C; Alcala I; Provansal M; Nguyen D; Nelidova D; Labernède G; Lubetzki J; Goulet R; Burban E; et al. Ectopic Expression of a Mechanosensitive Channel Confers Spatiotemporal Resolution to Ultrasound Stimulations of Neurons for Visual Restoration. Nat. Nanotechnol 2023, 18, 667–676. [PubMed: 37012508]

(23). Chen R; Romero G; Christiansen MG; Mohr A; Anikeeva P Wireless Magnetothermal Deep Brain Stimulation. Science 2015, 347, 1477–1480. [PubMed: 25765068]

(24). Sebesta C; Torres Hinojosa D; Wang B; Asfouri J; Li Z; Duret G; Jiang K; Xiao Z; Zhang L; Zhang Q; et al. Subsecond Multichannel Magnetic Control of Select Neural Circuits in Freely Moving Flies. Nat. Mater 2022, 21, 951–958. [PubMed: 35761060]

(25). Lee J-U; Shin W; Lim Y; Kim J; Kim WR; Kim H; Lee J-H; Cheon J Non-Contact Long-Range Magnetic Stimulation of Mechanosensitive Ion Channels in Freely Moving Animals. Nat. Mater 2021, 20, 1029–1036. [PubMed: 33510447]

(26). Xu K; Yang Y; Hu Z; Yue Y; Cui J; Culver JP; Bruchas MR; Chen H TRPV1-Mediated Sonogenetic Neuromodulation of Motor Cortex in Freely Moving Mice. J. Neural Eng 2023, 20, 016055.

(27). Huang Y-S; Fan C-H; Hsu N; Chiu N-H; Wu C-Y; Chang C-Y; Wu B-H; Hong S-R; Chang Y-C; Yan-Tang Wu A; et al. Sonogenetic Modulation of Cellular Activities Using an Engineered Auditory-Sensing Protein. Nano Lett. 2020, 20, 1089–1100. [PubMed: 31884787]

Author Manuscript Author Manuscript Author Manuscript Author Manuscript

(28). Cadoni S; Demené C; Provansal M; Nguyen D; Nelidova D; Labernede G; Alcala I; Lubetzki J; Goulet R; Burban E; et al. Sonogenetic Stimulation of the Brain at a Spatiotemporal Resolution Suitable for Vision Restoration. bioRxiv 2021, 2021.11.07.467597.

(29). Emiliani V; Entcheva E; Hedrich R; Hegemann P; Konrad KR; Löscher C; Mahn M; Pan Z-H; Sims RR; Vierock J; et al. Optogenetics for Light Control of Biological Systems. Nature Reviews Methods Primers 2022, 2, 1–25.

(30). Ou X; Qin X; Huang B; Zan J; Wu Q; Hong Z; Xie L; Bian H; Yi Z; Chen X; et al. High-Resolution X-Ray Luminescence Extension Imaging. Nature 2021, 590, 410–415. [PubMed: 33597760]

(31). Pei P; Chen Y; Sun C; Fan Y; Yang Y; Liu X; Lu L; Zhao M; Zhang H; Zhao D; et al. X-Ray-Activated Persistent Luminescence Nanomaterials for NIR-II Imaging. Nat. Nanotechnol 2021, 16, 1011–1018. [PubMed: 34112994]

(32). All AH; Zeng X; Teh DBL; Yi Z; Prasad A; Ishizuka T; Thakor N; Hiromu Y; Liu X Expanding the Toolbox of Upconversion Nanoparticles for In Vivo Optogenetics and Neuromodulation. Adv. Mater 2019, 31, e1803474. [PubMed: 31432555]

(33). Wang W; Tasset A; Pyatnitskiy I; Mohamed HG; Taniguchi R; Zhou R; Rana M; Lin P; Capocyan SLC; Bellamkonda A; et al. Ultrasound Triggered Organic Mechanoluminescence Materials. Adv. Drug Delivery Rev 2022, 186, 114343.

(34). Kim G; Lau VM; Halmes AJ; Oelze ML; Moore JS; Li KC High-Intensity Focused Ultrasound-Induced Mechanochemical Transduction in Synthetic Elastomers. Proc. Natl. Acad. Sci. U. S. A 2019, 116, 10214–10222. [PubMed: 31076556]

(35). Xu C; Huang J; Jiang Y; He S; Zhang C; Pu K Nanoparticles with Ultrasound-Induced Afterglow Luminescence for Tumour-Specific Theranostics. Nat. Biomed Eng 2023, 7, 298–312. [PubMed: 36550302]

(36). Kim G; Wu Q; Chu JL; Smith EJ; Oelze ML; Moore JS; Li KC Ultrasound Controlled Mechanophore Activation in Hydrogels for Cancer Therapy. Proc. Natl. Acad. Sci. U. S. A 2022, 119, e2109791119. [PubMed: 35046028]

(37). Yang F; Wu X; Cui H; Jiang S; Ou Z; Cai S; Hong G Palette of Rechargeable Mechanoluminescent Fluids Produced by a Biomineral-Inspired Suppressed Dissolution Approach. J. Am. Chem. Soc 2022, 144, 18406–18418. [PubMed: 36190898]

(38). Yang F; Wu X; Cui H; Ou Z; Jiang S; Cai S; Zhou Q; Wong BG; Huang H; Hong G A Biomineral-Inspired Approach of Synthesizing Colloidal Persistent Phosphors as a Multicolor, Intravital Light Source. Sci. Adv 2022, 8, eabo6743. [PubMed: 35905189]

(39). Wu X; Zhu X; Chong P; Liu J; Andre LN; Ong KS; Brinson K Jr; Mahdi AI; Li J; Fenno LE; et al. Sono-Optogenetics Facilitated by a Circulation-Delivered Rechargeable Light Source for Minimally Invasive Optogenetics. Proc. Natl. Acad. Sci. U. S. A 2019, 116, 26332–26342. [PubMed: 31811026]

(40). Yang F; Kim S-J; Wu X; Cui H; Hahn SK; Hong G Principles and Applications of Sono-Optogenetics. Adv. Drug Delivery Rev 2023, 194, 114711.

(41). Hong G. Seeing the Sound. Science 2020, 369, 638. [PubMed: 32764064]

(42). Wang W; Wu X; Kevin Tang KW; Pyatnitskiy I; Taniguchi R; Lin P; Zhou R; Capocyan SLC; Hong G; Wang H Ultrasound-Triggered In Situ Photon Emission for Noninvasive Optogenetics. J. Am. Chem. Soc 2023, 145, 1097–1107. [PubMed: 36606703]

(43). Xu C; He S; Wei X; Huang J; Xu M; Pu K Activatable Sonoafterglow Nanoprobes for T-Cell Imaging. Adv. Mater 2023, 35, e2211651. [PubMed: 37074842]

(44). Daiber A; Oelze M; August M; Wendt M; Sydow K; Wieboldt H; Kleschyov AL; Munzel T Detection of Superoxide and Peroxynitrite in Model Systems and Mitochondria by the Luminol Analogue L-012. Free Radic. Res 2004, 38, 259–269. [PubMed: 15129734]

(45). Yamaguchi S; Kishikawa N; Ohyama K; Ohba Y; Kohno M; Masuda T; Takadate A; Nakashima K; Kuroda N Evaluation of Chemiluminescence Reagents for Selective Detection of Reactive Oxygen Species. Anal. Chim. Acta 2010, 665, 74–78. [PubMed: 20381693]

(46). Liu L-H; Zhang Y-H; Qiu W-X; Zhang L; Gao F; Li B; Xu L; Fan J-X; Li Z-H; Zhang X-Z Dual-Stage Light Amplified Photodynamic Therapy against Hypoxic Tumor Based on an O2 Self-Sufficient Nanoplatform. Small 2017, 13, 1701621.

Author Manuscript Author Manuscript Author Manuscript Author Manuscript

(47). Kilic S; Toprak G; Ozdemir E Stability of CaCO3 in Ca(OH)2 Solution. Int. J. Miner. Process 2016, 147, 1–9.

(48). Wang W; Jiang S; Li S; Yan X; Liu S; Mao X; Yu X Functional Choline Phosphate Lipids for Enhanced Drug Delivery in Cancer Therapy. Chem. Mater 2021, 33, 774–781.

(49). Jiang S; Wang W; Dong L; Yan X; Li S; Mei W; Xie X; Zhang Y; Liu S; Yu X Infrared Responsive Choline Phosphate Lipids for Synergistic Cancer Therapy. Chemistry 2021, 27, 12589–12598. [PubMed: 34164858]

(50). Wang W; Lin L; Ma X; Wang B; Liu S; Yan X; Li S; Tian H; Yu X Light-Induced Hypoxia-Triggered Living Nanocarriers for Synergistic Cancer Therapy. ACS Appl. Mater. Interfaces 2018, 10, 19398–19407. [PubMed: 29781276]

(51). Jiménez-Pérez R; González-Rodríguez J; González-Sánchez M-I; Gómez-Monedero B; Valero E Highly Sensitive H2O2 Sensor Based on Poly(azure A)-Platinum Nanoparticles Deposited on Activated Screen Printed Carbon Electrodes. Sens. Actuators, B 2019, 298, 126878.

(52). Gomes A; Fernandes E; Lima JLFC Fluorescence Probes Used for Detection of Reactive Oxygen Species. J. Biochem. Biophys. Methods 2005, 65, 45–80. [PubMed: 16297980]

(53). Duco W; Grosso V; Zaccari D; Soltermann AT Generation of ROS Mediated by Mechanical Waves (ultrasound) and Its Possible Applications. Methods 2016, 109, 141–148. [PubMed: 27542338]

(54). Merényi G; Lind J; Eriksen TE Luminol Chemiluminescence: Chemistry, Excitation, Emitter. J. Biolumin. Chemilumin 1990, 5, 53–56. [PubMed: 2156408]

(55). Boyden ES; Zhang F; Bamberg E; Nagel G; Deisseroth K Millisecond-Timescale, Genetically Targeted Optical Control of Neural Activity. Nat. Neurosci 2005, 8, 1263–1268. [PubMed: 16116447]

(56). Stauffer PR; Paulides MM10.07 - Hyperthermia Therapy for Cancer. In Comprehensive Biomedical Physics; Brahme A, Ed.; Elsevier: Oxford, 2014; pp 115–151.

(57). Vernon MM; Lewin MChapter 53 - Fetal and Neonatal Echocardiography. In Avery's Diseases of the Newborn (Ninth ed.); Gleason CA; Devaskar SU, Eds.; W.B. Saunders: Philadelpia, 2012; pp 741–750.

(58). Finlayson L; Barnard IRM; McMillan L; Ibbotson SH; Brown CTA; Eadie E; Wood K Depth Penetration of Light into Skin as a Function of Wavelength from 200 to 1000 Nm. Photochem. Photobiol 2022, 98, 974–981. [PubMed: 34699624]

(59). Zhang F; Wang L-P; Brauner M; Liewald JF; Kay K; Watzke N; Wood PG; Bamberg E; Nagel G; Gottschalk A; et al. Multimodal Fast Optical Interrogation of Neural Circuitry. Nature 2007, 446, 633–639. [PubMed: 17410168]

(60). Vogt N. Sensing Calcium in Red. Nat. Methods 2016, 13, 468–468.

(61). Inoue M; Takeuchi A; Manita S; Horigane S-I; Sakamoto M; Kawakami R; Yamaguchi K; Otomo K; Yokoyama H; Kim R; et al. Rational Engineering of XCaMPs, a Multicolor GECI Suite for In Vivo Imaging of Complex Brain Circuit Dynamics. Cell 2019, 177, 1346–1360. [PubMed: 31080068]

(62). Klapoetke NC; Murata Y; Kim SS; Pulver SR; Birdsey-Benson A; Cho YK; Morimoto TK; Chuong AS; Carpenter EJ; Tian Z; et al. Independent Optical Excitation of Distinct Neural Populations. Nat. Methods 2014, 11, 338–346. [PubMed: 24509633]

(63). Lyu Y; Xie C; Chechetka SA; Miyako E; Pu K Semiconducting Polymer Nanobioconjugates for Targeted Photothermal Activation of Neurons. J. Am. Chem. Soc 2016, 138, 9049–9052. [PubMed: 27404507]

(64). Wu X; Yang F; Cai S; Pu K; Hong G Nanotransducer-Enabled Deep-Brain Neuromodulation with NIR-II Light. ACS Nano 2023, 17, 7941–7952. [PubMed: 37079455]

(65). Yang J-H; Kwan AC Secondary Motor Cortex: Broadcasting and Biasing Animal's Decisions through Long-Range Circuits. Int. Rev. Neurobiol 2021, 158, 443–470. [PubMed: 33785155]

(66). Kubanek J; Shukla P; Das A; Baccus SA; Goodman MB Ultrasound Elicits Behavioral Responses through Mechanical Effects on Neurons and Ion Channels in a Simple Nervous System. J. Neurosci 2018, 38, 3081–3091. [PubMed: 29463641]

Author Manuscript Author Manuscript Author Manuscript Author Manuscript

(67). Sato T; Shapiro MG; Tsao DY Ultrasonic Neuromodulation Causes Widespread Cortical Activation via an Indirect Auditory Mechanism. Neuron 2018, 98, 1031–1041. [PubMed: 29804920]

(68). Blackmore J; Shrivastava S; Sallet J; Butler CR; Cleveland RO Ultrasound Neuromodulation: A Review of Results, Mechanisms and Safety. Ultrasound Med. Biol 2019, 45, 1509–1536. [PubMed: 31109842]

(69). Yu K; Niu X; Krook-Magnuson E; He B Intrinsic Functional Neuron-Type Selectivity of Transcranial Focused Ultrasound Neuromodulation. Nat. Commun 2021, 12, 2519. [PubMed: 33947867]

(70). Cai J; Tong Q Anatomy and Function of Ventral Tegmental Area Glutamate Neurons. Front. Neural Circuits 2022, 16, 867053. [PubMed: 35669454]

(71). Rao S; Chen R; LaRocca AA; Christiansen MG; Senko AW; Shi CH; Chiang P-H; Varnavides G; Xue J; Zhou Y; et al. Remotely Controlled Chemomagnetic Modulation of Targeted Neural Circuits. Nat. Nanotechnol 2019, 14, 967–973. [PubMed: 31427746]

(72). Gu X; Song Q; Zhang Q; Huang M; Zheng M; Chen J; Wei D; Chen J; Wei X; Chen H; et al. Clearance of Two Organic Nanoparticles from the Brain via the Paravascular Pathway. J. Controlled Release 2020, 322, 31–41.

Author Manuscript Author Manuscript Author Manuscript Author Manuscript

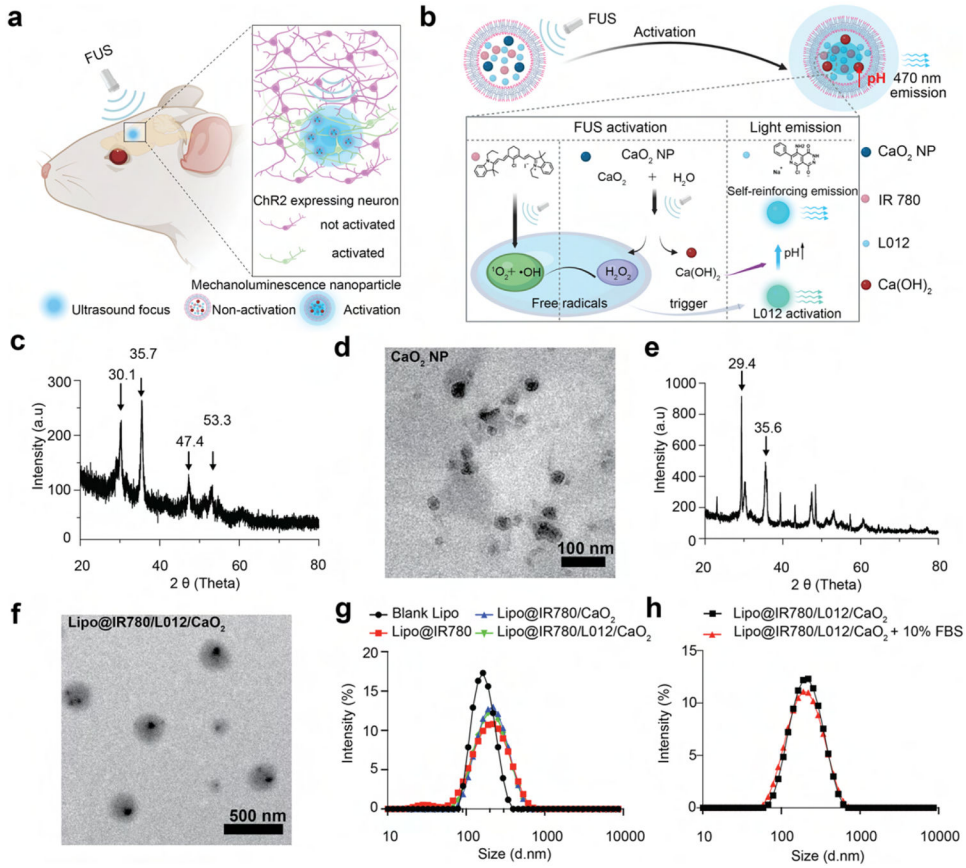

Figure 1.

FUS-activated nanotransducers act as a wireless light source for spatiotemporal neuromodulation. (a) Schematic of the neural activation through FUS-triggered blue light emission from Lipo@IR780/L012/CaO_2 mechanoluminescent liposomes at focus. (b) Mechanism of FUS-triggered light emission from cascaded mechanoluminescent nanoparticles. In this scheme, the ultrasound energy is absorbed through sonosensitizer IR780 to generate free radicals in the liposomes, and the ultrasound-induced mechanical force would also cause the perturbation of the polyethylene glycol (PEG) 200 coating at the CaO_2 surface, thus enlarging the reaction with H_2O to generate H_2O_2 and to increase the pH in the lumen due to the generation of $Ca(OH)_2$. Accelerated free radicals and H_2O_2 production react with L012 to generate blue light, and the increased pH would improve the quantum yield of L012, thus achieving enhanced blue light emission. (c) XRD analysis of PEG 200 coated CaO_2 nanoparticles. (d) TEM images of PEG 200 coated CaO_2 nanoparticles. (e) XRD analysis of PEG 200 coated CaO_2 nanoparticles after FUS stimulation. (f) TEM image of Lipo@IR780/L012/CaO_2 liposomes. (g) Dynamic light scattering (DLS) tests of blank and payload liposomes in solution. (h) Stability evaluation of payload liposomes in serum mimic solution tested by DLS.

Author Manuscript Author Manuscript Author Manuscript Author Manuscript

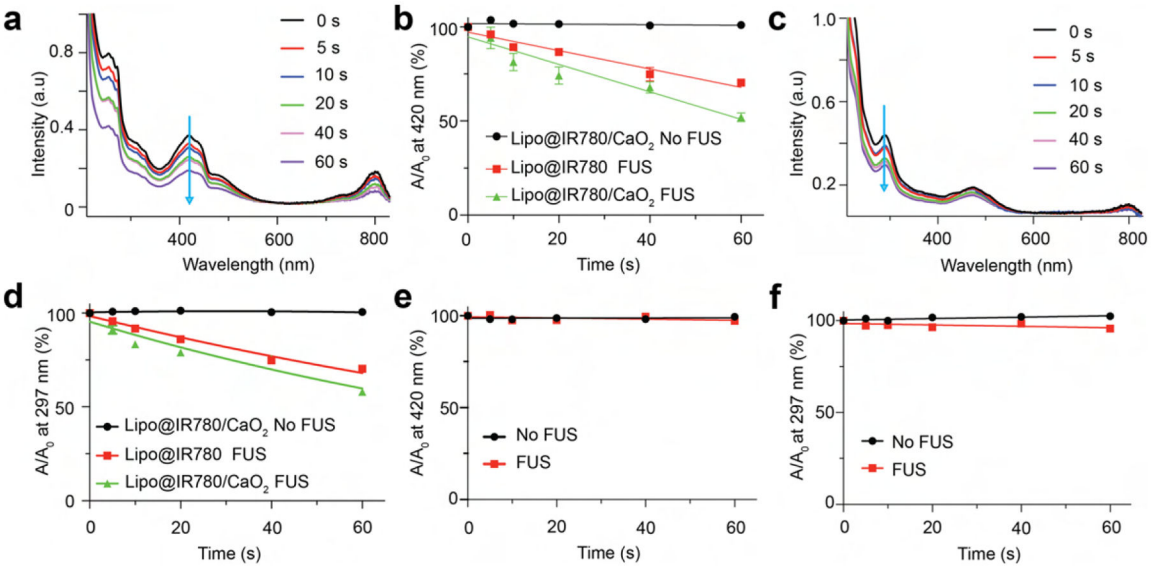

Figure 2.

FUS triggered the generation and consumption of free radicals by L012. (a) UV–vis spectra of DPBF under ultrasound irradiation (1.5 MHz, 1.55 MPa) over time, indicating the efficient generation of $^1O_2$. (b) Quantitative analysis of DPBF decomposition with or without ultrasound irradiation ($n > 3$ per group) in different nanoparticle solutions. (c) UV–vis spectra of SA under ultrasound irradiation (1.5 MHz, 1.55 MPa) over time. (d) Quantification analysis of SA decomposition with or without ultrasound irradiation ($n > 3$ per group) in different nanoparticle solutions. Quantification analysis of (e) DPBF decomposition and (f) SA decomposition at the similar irradiation conditions after loading L012 over time. These results showed an absence of free radical residues in Lipo@IR780/L012/CaO_2 liposomes under FUS irradiation.

Author Manuscript

Author Manuscript

Author Manuscript

Author Manuscript

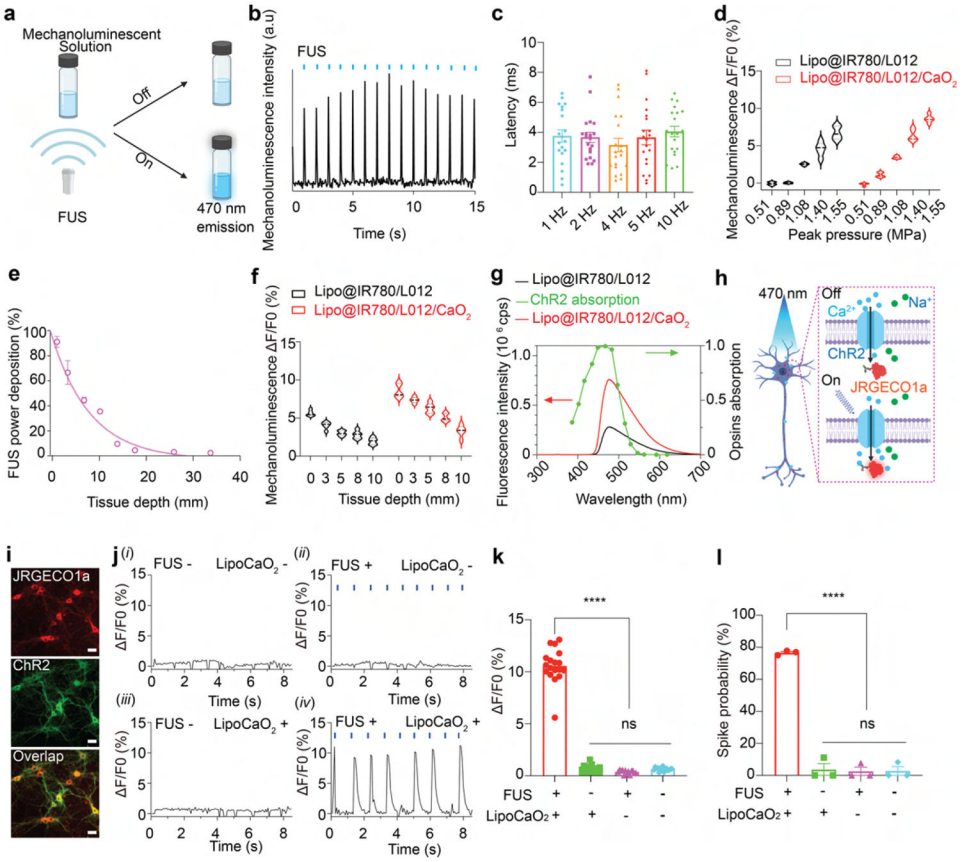

Figure 3.

FUS-triggered blue light emission and neuronal activation. (a) Schematic of the blue light emission from mechanoluminescence solution under ultrasound irradiation. (b) Photons were generated from Lipo@IR780/L012/CaO_2 liposomes under repetitive FUS irradiation (1.5 MHz, 1.55 MPa, pulse 50 ms on, 950 ms off). (c) Latency time between ultrasound excitation and photon emission from Lipo@IR780/L012/CaO_2 liposomes at different ultrasound irradiation frequencies. (d) Quantification analysis of light intensity from Lipo@IR780/L012 and Lipo@IR780/L012/CaO_2 liposomes under similar ultrasound irradiation (1.5 MHz, 1.55 MPa, pulse 50 ms on, 950 ms off). (e) Normalized ultrasound energy transmission efficiency in porcine skin (1.5 MHz, 1.55 MPa). (f) Quantification analysis of light intensity from Lipo@IR780/L012 and Lipo@IR780/L012/CaO_2 liposomes under similar ultrasound irradiation (1.5 MHz, 1.55 MPa, pulse 50 ms on, 950 ms off) at different tissue depths. (g) Mechanoluminescence spectra of Lipo@IR780/L012 and Lipo@IR780/L012/CaO_2 liposomes, where the emission spectrum of the liposomes is overlaid with the ChR2 opsin absorption spectrum (green dot curve). (h) Illustration of a ChR2-expressing neuron activating under ultrasound irradiation in the presence of Lipo@IR780/L012/CaO_2 nanoparticles. The ChR2 opsin channel could be activated under blue light emission. The Ca^{2+} imaging with JRGECO1a could be used to image the neuronal activation. (i) Fluorescent images of primary neurons expressing hSyn::ChR2-EYFP and hSyn::JRGECO1a; scale bar: 20 μm. (j) JRGECO1a fluorescence signal recording of ChR2-expressing neurons in different experimental conditions, (*i*) FUS −, $LipoCaO_2$ −; (*ii*) FUS +,

Author Manuscript Author Manuscript Author Manuscript Author Manuscript

$LipoCaO_2$ −; (*iii*) FUS −, $LipoCaO_2$ +; (*iv*) FUS +, $LipoCaO_2$ +, FUS stimulation (1.5 MHz, 1.55 MPa, pulse 100 on 900 ms off). (k) Statistical analysis of JRGECO1a signal changes in different groups ($n = 3$ per group, two-way ANOVA and multiple comparisons test). (l) Spike probability of ChR2-expressing primary neurons under the different conditions ($n = 3$ per group, two-way ANOVA and multiple comparisons test). All plots show mean ± SEM unless otherwise mentioned. *$P < 0.05$, **$P < 0.01$, ***$P < 0.001$, ****$P < 0.0001$; ns, not significant.

Author Manuscript Author Manuscript Author Manuscript Author Manuscript

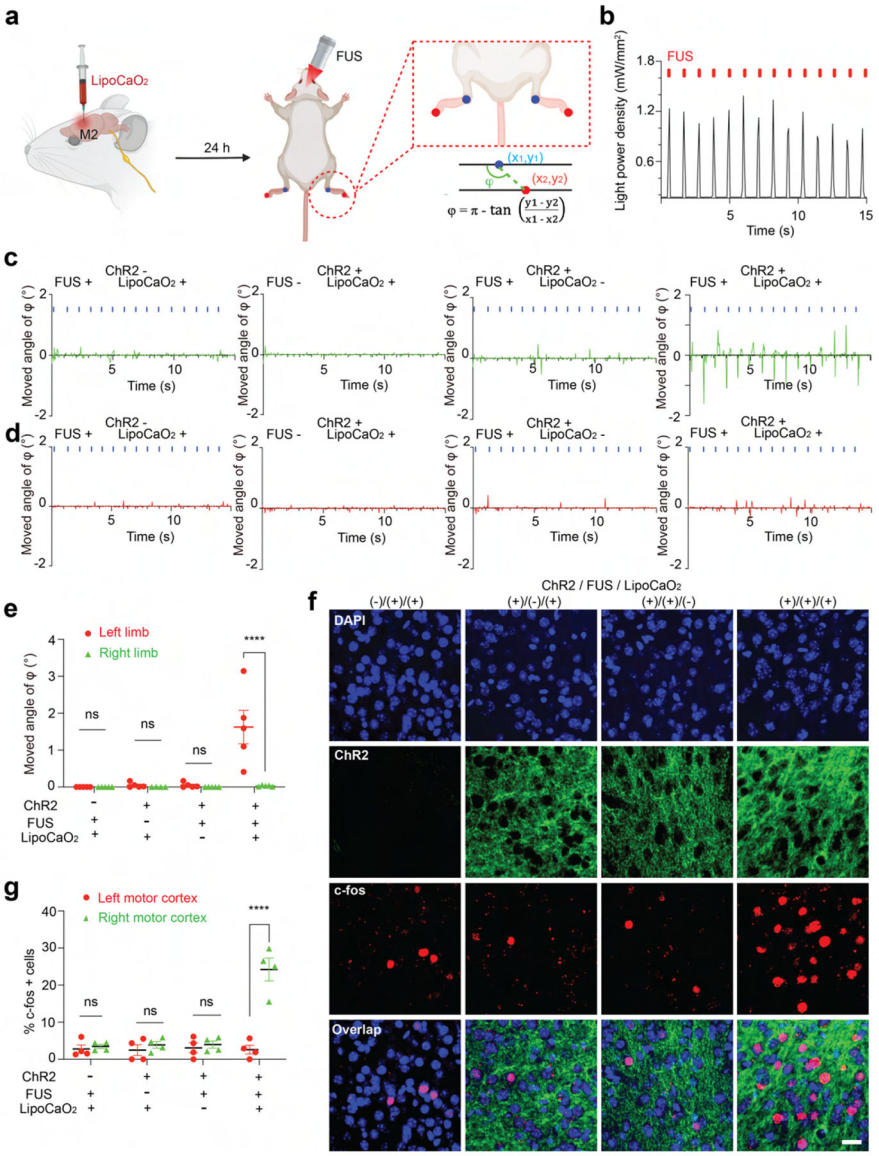

Figure 4.

In vivo sono-optogenetics for spatiotemporal motor cortex modulation. (a) Schematic of the remote motor cortex activation of sono-optogenetics for controlled limb motion. Lipo@IR780/L012/CaO_2 liposomes were injected into the M2 area in the right hemisphere. After 24 h, a FUS transducer with a focus on the motor cortex area was used to treat the mouse, and the limb motion was recorded via camera and analyzed with DeeplabCut. (b) Blue light emission from mechanoluminescent liposomes under the FUS irradiation (1.5 MHz, 1.55 MPa, pulse 100 on 900 ms off). (c) Time-resolved left limb motion and (d) right limb motion in different experimental conditions, FUS −, $LipoCaO_2$ −; FUS + , $LipoCaO_2$ −; FUS −, $LipoCaO_2$ +; and FUS +, $LipoCaO_2$ +. (e) Statistical analysis of the right and left limbs' motions in different groups of subjects (n = 5 per group, two-way ANOVA and multiple comparisons test) in response to FUS irradiation. (f) Confocal images of the right motor cortex region under different experimental conditions. Increased c-Fos

Author Manuscript Author Manuscript Author Manuscript Author Manuscript

signals triggered by FUS were only observed in the presence of both ChR2 opsins and mechanoluminescent liposomes; scale bar: 20 μm. (g) Statistical analysis of c-Fos signal densities under different experimental conditions at the M2 motor cortex region ($n = 4$ per group, two-way ANOVA, and multiple comparisons test). All plots show mean ± SEM unless otherwise mentioned. *$P < 0.05$, **$P < 0.01$, ***$P < 0.001$, ****$P < 0.0001$; ns, not significant.

Author Manuscript Author Manuscript Author Manuscript Author Manuscript

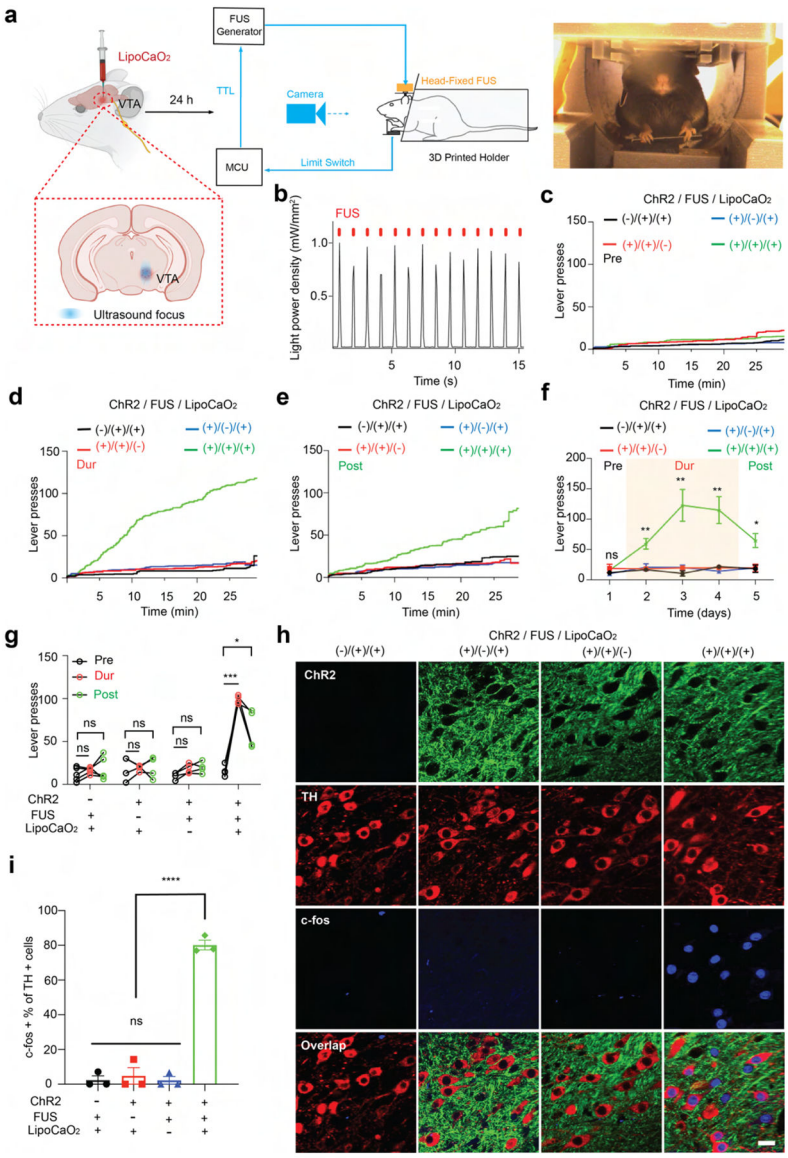

Figure 5.

In vivo sono-optogenetics for spatiotemporal mouse VTA modulation. (a) Schematic of the remote VTA neuron activation of sono-optogenetics for lever press tests. Once the mouse presses the lever trigger, a FUS pulse is given (1.5 MHz, 1.55 MPa, pulse 100 ms). (b) The blue light emission from mechanoluminescence liposomes under FUS irradiation (1.5 MHz, 1.55 MPa, pulse 100 on 900 ms off). (c) The mouse-lever-press curve at the prestimulus session, where the FUS generator was off to obtain the lever press baseline, (d) during FUS stimulation (or no FUS stimulation) epoch, where FUS is triggered on via the action of the mouse, and (e) at poststimulus epoch (FUS generator is off) under the different experimental conditions (n = 4 per group, 1.5 MHz, 1.55 MPa, pulse 100 ms). (f) Time courses of the total lever presses in each epoch for the mouse under the different experimental conditions (n = 4 per group; 1.5 MHz, 1.55 MPa, pulse 100 ms; two-way ANOVA and multiple comparisons test). (g) Statistical analysis of mouse lever presses at all epochs (n = 4 per group; two-way

Author Manuscript Author Manuscript Author Manuscript Author Manuscript

ANOVA and multiple comparisons test). (h) Confocal images of the VTA region under the different experimental conditions. Increased c-Fos signals triggered by FUS were only observed in the presence of both ChR2 opsins and mechanoluminescent liposomes; scale bar: 20 μm. (i) Statistical analysis of c-Fos signal densities under the different experimental conditions at the VTA region ($n = 4$ per group, two-way ANOVA, and multiple comparisons test). All plots show mean ± SEM unless otherwise mentioned. *$P < 0.05$, **$P < 0.01$, ***$P < 0.001$, ****$P < 0.0001$; ns, not significant.

Author Manuscript Author Manuscript Author Manuscript Author Manuscript

Table 1.

DLS Tests and DLC Determinations of Different Liposome Solutions

entry	nanoparticles	size (*d*, nm)	PDI	zeta potential (mV)	DLC of IR780 (wt %)	DLC of L012 (wt %)
1	Blank Lipo	166.9 ± 5.9	0.174	−26.0 ± 0.2	N/A	N/A
2	Lipo@IR780	168.8 ± 0.8	0.236	−10.2 ± 0.1	5.70 ± 0.46	N/A
3	Lipo@IR780/L012	173.3 ± 2.3	0.228	−10.5 ± 0.4	5.70 ± 0.20	6.0 ± 0.5
4	Lipo@IR780/CaO2	177.8 ± 1.4	0.210	−11.2 ± 0.2	5.83 ± 0.61	N/A
5	Lipo@IR780/CaO2/L012	175.9 ± 0.6	0.217	−10.9 ± 0.2	5.73 ± 0.47	6.17 ± 0.31
6	Lipo@IR780/CaO2/L012 + 10% FBS	177.9 ± 3.1	0.233	N/A	N/A	N/A